Chapter 6

Photophysical Characterization of Pentacoordinated Compounds

6.1 Photophysical properties of Q'_2GaL^n compounds

Gallium coordination compounds obtained with mono and bidentate ligands were characterized in dichloromethane solutions. Photoluminescent quantum yields, Φ_{PL}, were calculated using $[Ru(bipy)_3]Cl_2$, (bipy= 2,2′-bipyridine) (H_2O, Φ_{PL}= 0,028) as standard. Absorption and emission spectra of **Q'_2GaL^n** gallium complexes, described in **Figure 6.1**, were collected in dichloromethane solutions, on KBr pellets and on amorphous thin films obtained by spin coating techniques.

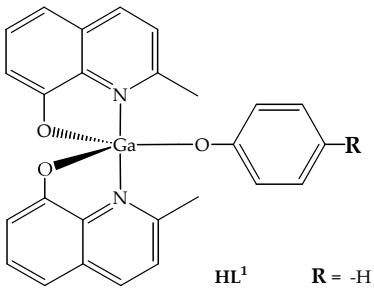

Q'_2GaL^n

HL^1 R = -H

HL^2 -CN

HL^3 $-NO_2$

HQ' = 2-methyl-8-hydroxyquinoline

Figure 6.1: Q'_2GaL^n compounds.

The recorded absorption and emission spectra in solution illustrated in **Figure 6.2** show almost the same spectral profile for **$Q'_2GaOC_6H_5$**, **$Q'_2GaOC_6H_4CN$** compounds with an intense band at 260 nm and 365 nm attributed to a $\pi \rightarrow \pi^*$ transitions, and two shoulders at 304 nm and 315 nm, while in **$Q'_2GaOC_6H_4NO_2$** the intense the shoulder at 304 nm became an intense band.

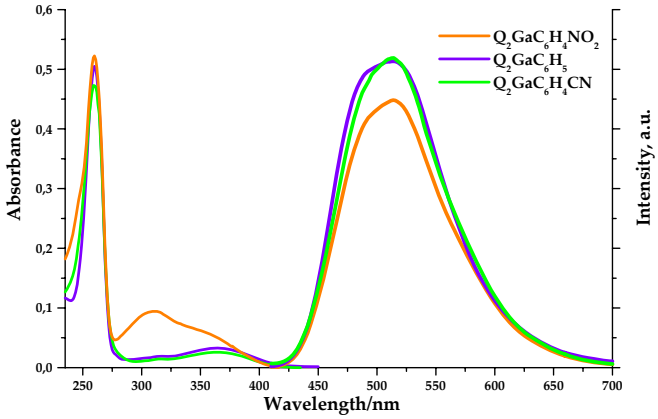

Figure 6.2: *absorption and emission spectra of* ***Q'₂GaOC₆H₅, Q'₂GaOC₆H₄CN, Q'₂GaOC₆H₄NO₂.***

Emission spectra were collected exciting the dichloromethane solutions at 365 nm to obtain maximum emission band values at 507-518 nm range as reported in **Table 6.1**. All compounds show high photoluminescence quantum yields with values of about 40% for **Q'₂GaOC₆H₅** and **Q'₂GaOC₆H₄CN** compounds and 25% for **Q'₂GaOC₆H₄NO₂** compound.

In particular, while for phenol and *p*-cyanophenol derivatives the Φ_{PL} values are almost independent from the exciting wavelength in the range 290-410 nm, for *p*-nitrophenol derivative, which absorption spectrum shows a prominent band at 304 nm, the emission quantum yield measured exciting at this wavelength is dramatically reduced at 5%. The spectral characteristics showed in solution by this series of complexes, are retained in solid and film samples. As reported in **Table 6.1**, the absorption bands collected on KBr pellets are red-shifted respect those registered in solution, the film emission is slightly blue-shifted a reduced Stokes shift is noted in the solid samples. Although the emission spectra show the same profile, the emission maximum of gallium compounds obtained with *para* substituted phenols, registered both in solution and in KBr pellets, are red-shifted about 10 nm respect to the emission of gallium compound synthesised with the unsubstituted phenol.

Q'_2GaL^n	CH_2Cl_2 solutions		KBr pellets		Films	
	Absorbance λ/nm, ($\varepsilon/M^{-1}cm^{-1}$)	Emission λ/nm, $^a\Phi_{PL}$	Absorbance λ/nm	Emission λ/nm	Absorbance λ/nm	Emission λ/nm
$Q'_2GaOC_6H_5$	260(67000) 304(sh) - 315(sh) 365(4500)	507, (0.40)	265 315(sh) - 380	472	264 320(sh) - 362	508
$Q'_2GaOC_6H_4CN$	260(68370) 304(sh) - 315(sh) 365(2930)	518, (0.44)	264 305(sh) - 375	480	261 315(sh) - 368	500
$Q'_2GaOC_6H_4NO_2$	260(68970) 304(11800),365(sh)	514, (0.25) 514, (0.05)^b	263 340	480	263 318 - 340	500

$^a\lambda_{ex}$ = 365 nm, $^b\lambda_{ex}$ = 304 nm

Table 6.1: *Q'_2GaL^n absorption, emission and Φ_{PL} in CH_2Cl_2 solutions in KBr pellets and on film.*

Comparing the electronic spectra of this series of complexes with those of similar pentacoordinated quinolinate gallium derivatives obtained different monodentate ligands no appreciable differences can be found.[1,2] This is an evidence of the fact that electronic properties of this class of complexes are mainly due to the quinolinate ligands.

6.1.1 Theoretical calculations and HOMO-LUMO assignments

The structure of the ground and excited state, electron transition and the energy transfer mechanism influence the luminescence and the electroluminescence of the metal chelate so theoretical calculation were carried out in order to understand the nature of the electronic structure of **Q'_2GaL^n** series.

B3LYP/6-31G(d) computations have been applied to these pentacoordinated gallium(III) complexes after ground state energy minimization. **Figure 6.3** shows the Kohn-Sham (KS) orbital energies and shapes of some of the highest occupied and lowest unoccupied orbitals of **$Q'_2GaOC_6H_5$**. Their qualitative description can be extended to **$Q'_2GaOC_6H_4CN$** and **$Q'_2GaOC_6H_4NO_2$**.

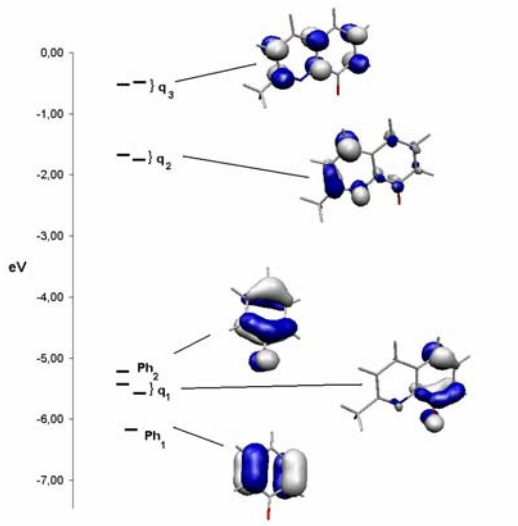

Figure 6.3: *description of* ***Q'$_2$GaOC$_6$H$_5$*** *complex Kohn-Sham orbitals close in energy to the HOMO and the LUMO.*

A general feature of all the reported orbitals is the substantial localization on the ligands, with a very small contribution from the metal centre. This is a typical feature of this class of compounds and it has already pointed out in the cases of AlQ_3, ZnQ_2 and AlQ'_2L.[3,8] The orbitals reported in **Figure 6.3** can be grouped in orbitals localized on the Q' chelants and orbitals localized on the L^n ligand. The Q' orbitals have been labeled as "q" and consist in couples of almost-degenerate orbitals, which are mostly produced by the slightly interacting Q' fragment orbitals, delocalized on both the chelants. The L^n orbitals have been labeled as "p" orbitals, and they are very similar to the fragment orbitals of the pyridyl-fused phenolate moiety.

Figure 6.3 shows the fragment orbitals that can be assigned to each KS orbital in this gallium pentacoordinate compounds series.

It is possible to note that, in the case of **Q'$_2$GaOC$_6$H$_5$** (**1**), the HOMO is localized on L^1 (p_2), while the LUMO is localized on the Q' ligands (q_2). This characteristic is not retained in the case of **Q'$_2$GaOC$_6$H$_4$CN** (**2**) and **Q'$_2$GaOC$_6$H$_4$NO$_2$** (**3**). **Figure 6.4** shows the energy trend of these orbitals in **Q'$_2$GaL^n** series.

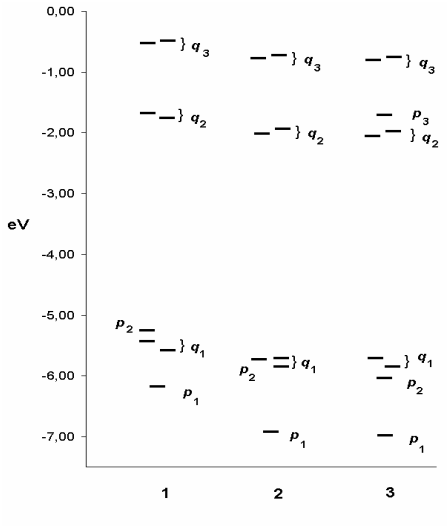

Figure 6.4: *energy level scheme of relevant Kohn-Sham orbitals of* ***Q′₂GaLⁿ*** *complexes.*

The presence of the electron attracting groups -CN and -NO_2 in the L^2 and L^3 ligands, leads to a stabilization of the p orbitals. As a consequence, in **2** and **3** the HOMO becomes localized on the Q′ chelants (one of the q_1 orbitals), whereas the LUMO continues to be a q_2 localised orbital. In the case of compound **3**, the virtual orbital p_3 (not reported in the case of compounds **1** and **2**) is computed. It consists in a π orbital with antibonding character located between the oxygen and nitrogen atoms of the -NO_2 group. **Table 6.2** collects the energies of the reported orbitals.

Q′₂GaOC₆H₅		***Q′₂GaOC₆H₄CN***		***Q′₂GaOC₆H₄NO₂***	
p_1	-6.20	p_1	-6.92	p_1	-6.99
q_1	-5.59	q_1	-5.84	p_2	-5.98
q_1	-5.45	p_2	-5.73	q_1	-5.88
p_2 *(HOMO)*	-5.20	q_1 *(HOMO)*	-5.70	q_1 *(HOMO)*	-5.73
q_2 *(LUMO)*	-1.77	q_2 *(LUMO)*	-2.02	q_2 *(LUMO)*	-2.05
q_2	-1.69	q_2	-1.94	q_2	-1.97
q_3	-0.54	q_3	-0.77	p_3	-1.65
q_3	-0.50	q_3	-0.74	q_3	-0.80
				q_3	-0.77

Table 6.2: *energies of the Kohn-Sham orbitals reported in* ***Figures 6.3*** *and* ***6.4****. All the values are in eV.*

The presence of the p_3 orbital is important to understand the absorption spectrum of this compound, somehow different from those of **1** and **2**.

According to TD-DFT computations, the electronic spectra of the three compounds show two principal absorptions. The first absorption is computed at 399 nm (3.10 eV) for **1** and 400 nm (3.10 eV) for **2** and **3**, while the second one is more intense and in all cases is found between 242 and 247 nm (5.11 - 5.01 eV). These electronic transitions can be assigned to changes in the electronic density within the Q' chelants and, in this sense, can be considered localized on these chelants. In the case of **3**, the presence of the $-NO_2$ group leads to an intense additional absorption computed at 304 nm (4.08 eV) associated to an electronic transition from the p_2 quinolinate-localized orbital to the p_3 orbital localized on the $-NO_2$ group. The computed spectrum well reproduces the experimental one, allowing an accurate peak attribution. **Table 6.3** reports information about the six lowest energy excited states. These states can be classified in two classes: q-localized and p→q charge transfer.

$Q'_2GaOC_6H_5$			$Q'_2GaOC_6H_4CN$			$Q'_2GaOC_6H_4NO_2$		
State	***Wavelength (f)[a]***	***Composition***	***State***	***Wavelength (f)[a]***	***Composition***	***State***	***Wavelength (f)[a]***	***Composition***
S1	434 nm (0.0007)	p_2-q_2	***S1***	400 nm (0.0805)	q_1-q_2	***S1***	400 nm (0.0809)	q_1-q_2
S2	417 nm (0.0005)	p_2-q_2	***S2***	392 nm (0.0049)	p_2-q_2	***S2***	390 nm (0.0091)	q_1-q_2
S3	399 nm (0.0819)	q_1-q_2	***S3***	388 nm (0.0031)	mixed q_1-q_2 and p_2-q_2	***S3***	377 nm (0.0038)	q_1-q_2
S4	389 nm (0.0052)	q_1-q_2	***S4***	378 nm (0.0019)	p_2-q_2	***S4***	369 nm (0.0029)	q_1-q_2
S5	378 nm (0.0044)	q_1-q_2	***S5***	377 nm (0.0039)	q_1-q_2	***S5***	368 nm (0.0007)	p_2-q_2
S6	370 nm (0.0040)	q_1-q_2	***S6***	368 nm (0.0042)	q_1-q_2	***S6***	356 nm (0.0045)	p_2-q_2
S7	317 nm (0.0001)	p_1-q_1	***S7***	296 nm (0.0016)	q_1-q_3 plus other ones	***S7***	334 nm (0.0003)	q_1-p_3

[a] *f: oscillator strength*

Table 6.3: *the computed lowest-energy excited states of compounds **1**-**3**. The reported composition has to be considered a qualitative description in terms of monoelectronic excitation.*

Interestingly, in the case of compound **1**, the excited states S_1 and S_2 belong to the p→q charge transfer class, with low oscillator strengths. These transitions can be assigned to monoelectronic excitations from the p_2 to the q_2 orbital. On

the other hand, the excited state S_3 is a q-localized transition ($q_1 \rightarrow q_2$ monoelectronic excitations) with larger oscillator strength. Thus, according to the computations, the experimental lowest-energy absorption band should not be associated to the HOMO-LUMO transition. This is the only difference among **1** and both compounds **2** and **3**, for which the first excited state is a $q_1 \rightarrow q_2$ transition with larger oscillator strength. Furthermore, the first intense computed excitation at 399-400 nm for **1-3** is always a $q_1 \rightarrow q_2$ transition, as proved by the constant energy gap between q_1 and q_2 orbitals, of 3.68 eV in all compounds. We can conclude that the substituents on the L^n ligands do not significantly influence the electronic structure of the Q' chelants, leaving the q-localized electronic transitions within an extremely narrow interval of wavelength. A similar observation can be extended to the fluorescence process. The experimental similarity in the fluorescence peak wavelengths of the three complexes can be explained as a consequence of the localisation of the emissive electronic transitions on the Q' chelants. As reported in **Table 6.3**, the lowest energy excited state (S_1) in complex **1** should produce a significantly different emission wavelength peak and quantum yield respect to the other complexes. In fact, the S_1 energy (relative to the ground state) changes from 2.86 eV (434 nm) in complex **1** to 3.09 eV (400 nm) in complexes **2** and **3**. This gap of 0.23 eV is not confirmed by our experiments, where the fluorescence emission peak spreads in a range of 0.06 eV in CH_2Cl_2 solution, 0.05 eV in KBr pellets and 0.04 eV in solid films (**Table 6.4**).

Q'_2GaL^n	CH_2Cl_2 solution [a]Emission λ/nm, eV (Φ_{PL})	KBr pellets Emission λ/nm, eV	Film Emission λ/nm, eV
$Q'_2GaOC_6H_5$	507, 2.45 (0.40)	472, 2.63	508, 2.44
$Q'_2GaOC_6H_4CN$	518, 2.39 (0.45)	480, 2.58	500, 2.48
$Q'_2GaOC_6H_4NO_2$	514, 2.41 (0.25)	480, 2.58	500, 2.48

λ_{ex}= 365 nm

Table 6.4: *emission photophysical data of* Q'_2GaL^n

Furthermore, the shape of the emission peaks (**Figure 6.2**) is comparable for all complexes, proving a similarity in the emission processes. The extremely low oscillator strength assigned to the S_1 state of complex **1** should imply a barely emissive complex, which does not correspond to the experimental data. Therefore we can conclude that the emission process as well as the lowest-energy absorption processes are dominated by the Q' chelants. A strong evidence of the predominance of the Q' chelants in the fluorescence process has already been observed in the case of similar pentacoordinated aluminum complexes[3] for which a low energy monodentate phenolate→quinolinate excited state is present. As a consequence of this finding, after light absorption and population of the $q_1 \rightarrow q_2$ excited states (from S_3 to S_6 in complex **1**), the non-radiative internal conversion towards the S_1 state is slower than the emission from the populated (pumped) states, which is in agreement with the apparent low electronic interaction between the L^n ligands and Q' chelants previously discussed. With reference to the absorption spectra, the presence of an intense electronic excitation around 304 nm, assigned to the $p_2 \rightarrow p_3$ transition involving the -NO_2 chromophore, is the only relevant difference between complexes **1-2** and complex **3**. As already reported in the discussion of the experimental spectra, this band seems to be overlapped with the lowest energy band at 365 nm (**Figure 6.2**), which is attributed to $q_1 \rightarrow q_2$ excitations. This evidence could explain the lowest quantum yield observed in the case of complex **3**. The lowest population of the emissive Q'-localised excited states, combined with a small interaction between the L^n and Q' ligands (with consequent slow intersystem crossing towards the emissive state) could lead to a reduced quantum yield. This is supported by the different **Φ**-value of **3** measured exciting the complex on the band corresponding to the $p_2 \rightarrow p_3$ (304 nm) or to the $q_1 \rightarrow q_2$ (365 nm) transition. This limitation should not be encountered in electroluminescence

experiments, when the population of the excited states is achieved by hole-electron recombination only mediated by the Q' chelants.

6.1.2 Absolute photoluminescence efficiency on film

Absolute photoluminescence quantum yield (PLQY) on film were calculated in the Organic Semiconductor Centre laboratories of the Physic and Astronomy Department of the University of St. Andrews under the supervision of professor Ifor D. W. Samuel.

The measurement were collected under ambient and dark conditions with an integrating sphere (**Figure 6.5**) coupled with a silicon photodiode.

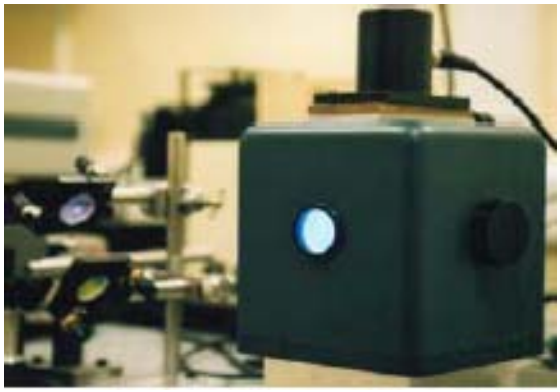

Figure 6.5: *integrating sphere.*

The excitation source was a He – Cd LASER with an excitation wavelength of 325 nm. The integrating sphere is a hollow sphere, 10 cm diameter, coated on the inside walls with a diffusely reflecting material, **Scheme 6.1**. The flux of light received through an aperture in the sphere is proportional to the total amount produced within the sphere independently of its angular distribution.

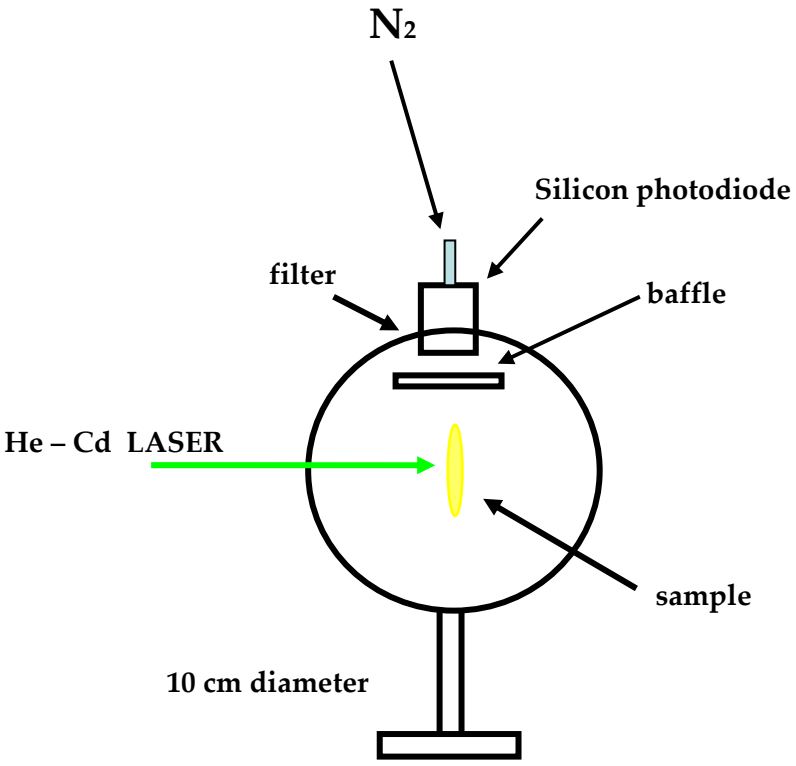

Scheme 6.1: *schematic representation of the integrating sphere.*

For each compound were prepared two samples and for each samples were collected two measurements. All compounds were characterized four times. After measurement with the integrating sphere, the photoluminescence spectra of the films were recorded with a fluorimeter. The obtained PLQY is the average value of four calculated results.

Films on quartz discs (1 cm diameter, 1 mm thickness) of each compound were obtained by spin-coating (speed: 2500 rpm, ramp: 50 rpm, dwell: 50 sec) from chloroform solutions (10 mg, 0,5 mL). The calculations were obtained following the method proposed by Greenam *et al.*.[9]

In the **Figure 6.6** is illustrated the experimental set-up adopted for thiskind of measurements. With the photodiode is measured the laser incident signal power $\mathbf{X}_{\text{LASER}}$, without filter and sample. Then the laser power on sample $\mathbf{X}_{\text{sample}}$, and the laser power on the sphere wall $\mathbf{X}_{\text{sphere}}$, were collected in the presence of

the filter and the sample. The transmitted ray **T** from the sample is checked using a power meter.

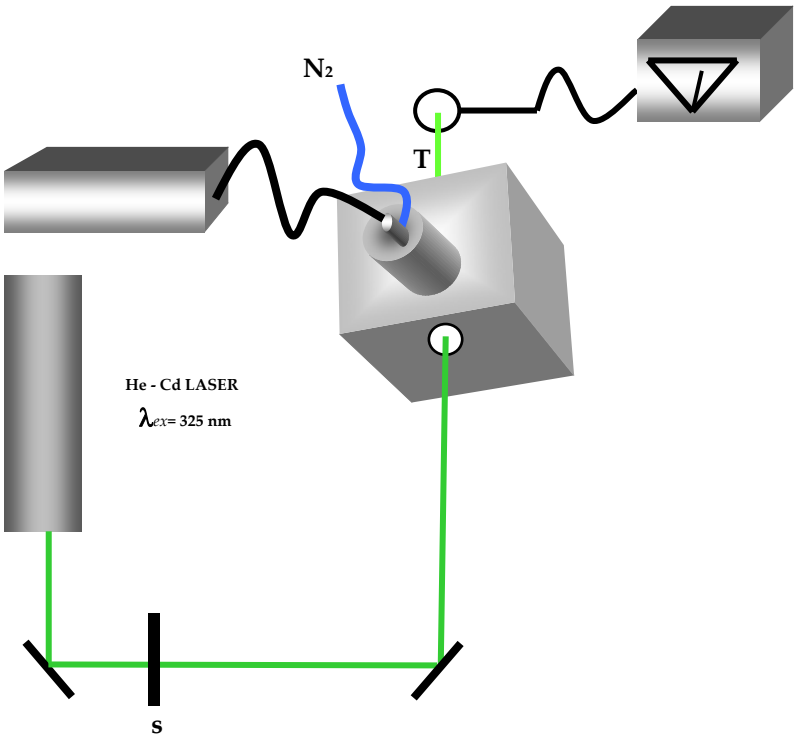

Figure 6.6: *experimental set-up.*

For each sample were collected two reflective index **R**, by checking the reflected ray from the sample with a power meter, the angular distribution of the emitted light is highly sensitive to refractive index of the material and to the orientation of emitting dipoles within the film.[10] After measurements with a fluorimeter the photoluminescent spectra **L**(λ) of the films were collected. The experimental set-up is illustrated in **Figure 6.7**.

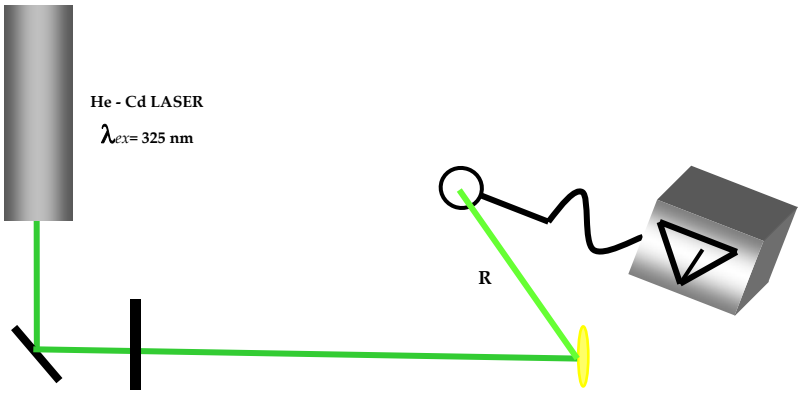

Figure 6.7: *experimental set-up to collect reflective index.*

Then all collected values were used to calculate the quantum efficiency with the **Equations 6.1** representing the ratio of the emitted photon number to absorbed photon number.

$$X = \frac{X_{sample} - (R + T)\, X_{sphere}}{(1 - R - T)\, X_{LASER}} \quad \textit{quantum efficiency}$$

X_{sample} = *LASER on sample*

X_{sphere} = *LASER on the sphere wall*

X_{LASER} = *LASER incident signal without filter*

R = *reflectance*

T = *trasmittance*

Equations 6.1: *quantum efficiency.*

While with **Equation 6.2** was calculated the correction factor for the spectral response influenced by the technical limit of each component of the sphere set-up.

$$Y = \int \frac{S_{sphere}(\lambda)\, L(\lambda) G(\lambda) F(\lambda)}{S_{lamp}(\lambda)}\, d\lambda \times \left(\frac{S_{sphere}(\lambda_{ex})\, G(\lambda_{ex})}{S_{lamp}(\lambda_{ex})} \int L(\lambda)\, d\lambda \right)$$

correction factor for the spectral response

S_{sphere} = *spectral responce of the sphere*

S_{lamp} = *spectrum of the lamp*

$F(\lambda)$= *trasmission of the filter*

$L(\lambda)$= *emission spectrum*

$G(\lambda)$= *quantum efficiency of the photodiode*

Equations 6.2: *correction factor.*

The absolute photoluminescence quantum yield is given by **X/Y**. Then emission spectra on film of all compounds, reported in **Figure 6.8**, were recorded.

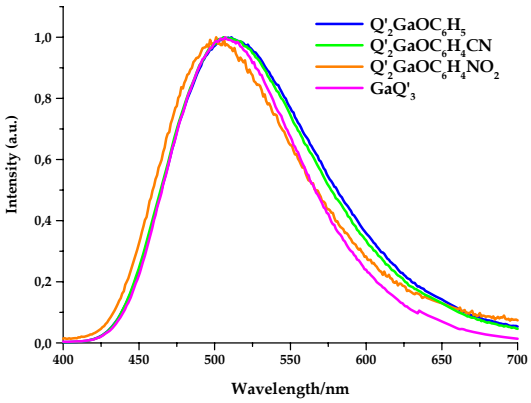

Figure 6.8: *emission spectra on film.*

GaQ$_3$ complex was also taken in account as reference compounds, so the calculated PLQY on film are illustrated in the **Table 6.5**.

Compounds	*Emission* λ_{max}*/nm*	Φ_{PL}
GaQ'$_3$	507	18%
Q'$_2$GaOC$_6$H$_5$	507	28%
Q'$_2$GaOC$_6$H$_4$CN	506	31%
Q'$_2$GaOC$_6$H$_4$NO$_2$	500	1,8%

Table 6.5: *emission maximum and absolute photoluminescence quantum yield.*

As can be evidenced the absolute quantum efficiency of **Q'$_2$GaOC$_6$H$_4$NO$_2$** complex is dramatically reduced.

6.1.3 Blended films with TPD and TPBI

A series of characterizations on film were carried out in order to have an idea about the charge transport capability of the synthesised gallium compounds.

Thin films obtained by spin-coating from dichloromethane solutions of gallium compounds blended with charge transport materials in different percent in weight were taken in account. For this purpose TPD or TPBI, often exploited in multilayer device structure, were chosen.

Therefore dichloromethane solutions (10 mg, 0.5 mL) of gallium compounds were prepared in which TPD and TPBI was dissolved in 10, 20 and 50 percent in weight. The films were realized adopting the same spin-coating parameters (2500 speed, 50 ramp, 50 dwell) used for the calculation of the absolute photoluminescence efficiencies previously described. The excitation wavelength λ_{ex} was 325 nm.

6.1.3.1 Photophysical behaviour of TPD and TPBI.

TPD, which molecular structure is illustrated in **Figure 6.9**, is known as hole transporting material.[11] The photophysical properties in dichloromethane solution are reported in **Figure 6.10**.

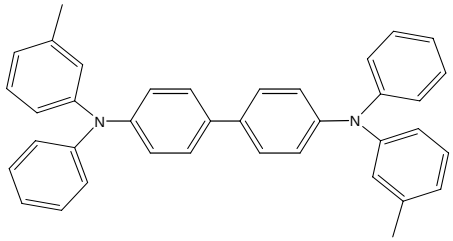

Figure 6.9: *TPD; N,N′-diphenyl-N,N′-bis(3-methylphenyl)-1,1′-biphenyl-4,4′-diamine.*

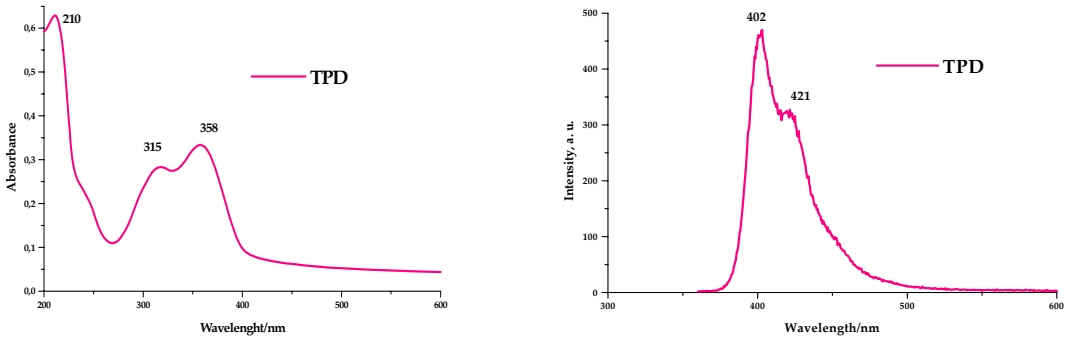

Figure 6.10: *absorption and emission spectra on film of TPD.*

Instead, TPBI is an electron transport material.[12] **Figure 6.11** report the molecular structure while the absorption and the emission spectra, collected in dichloromethane solution, are illustrated in **Figure 6.12**.

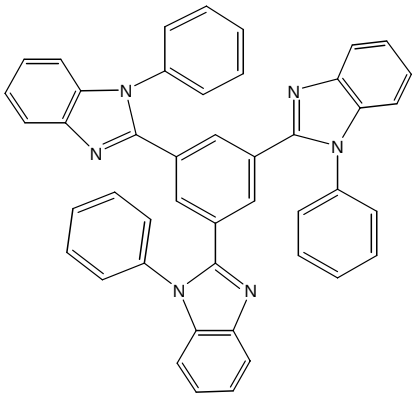

Figure 6.11: *TPBI; 1,3,5-tri(phenyl-2-benzimidazole)-benzene.*

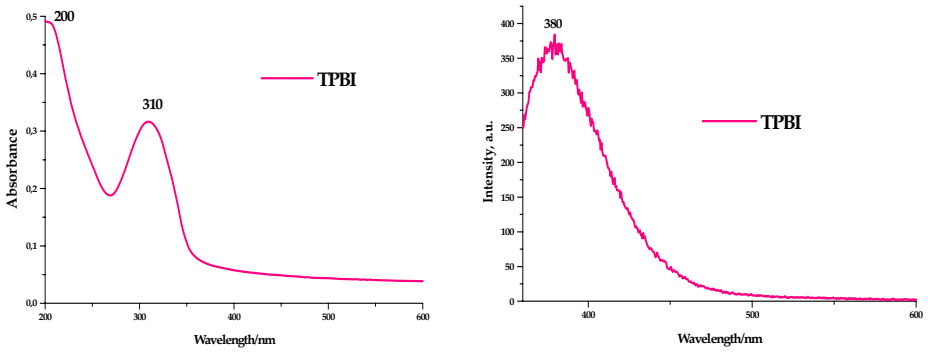

Figure 6.12: *absorption and emission spectra on film of TPBI.*

6.1.3.2 Blended film with TPD

Figure 6.13 report the absorption and the emission spectra of **Q'$_2$GaOC$_6$H$_5$** blended with TPD in 10, 20 and 50 percent in weight. In the absorption spectra only the bands at 310 nm and at 360 nm show the contribution of the TPD. While the emission spectra show an enhancement of the emission intensity by increasing the TPD amount. Probably this phenomenon is due to an energy

transfer mechanism between TPD and **Q′$_2$GaOC$_6$H$_5$**. The intense TPD emission disappear.

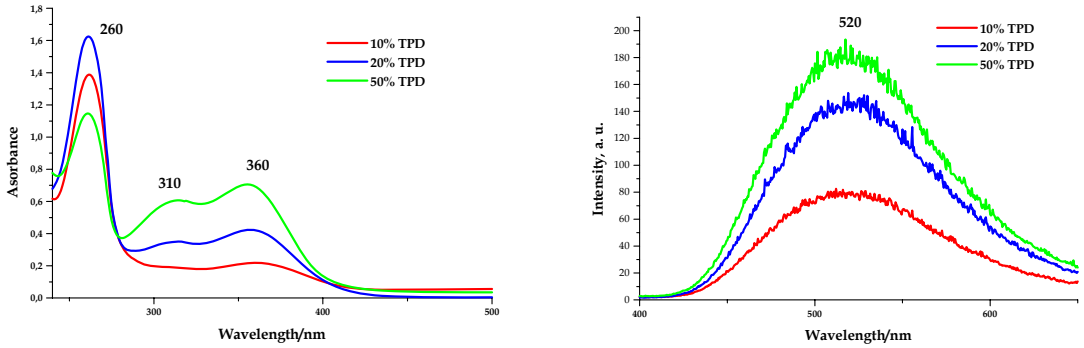

***Figure 6.13**: absorption and emission spectra on film of **Q′$_2$GaOC$_6$H$_5$**:TPD blend.*

Instead the absorption and the emission spectra on film of **Q′$_2$GaOC$_6$H$_4$CN** blended with TPD reported in **Figure 6.14**, show very weak contribution of TPD in the absorption spectra and a quenching effect of the emission intensity by increasing the TPD amount.

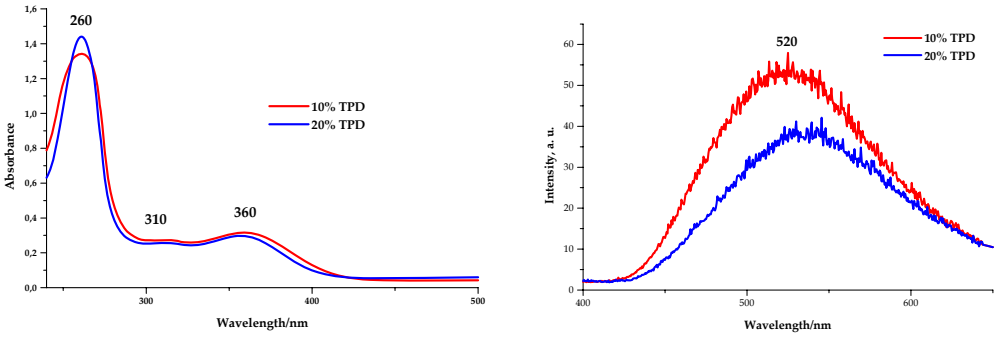

***Figure 6.14:** absorption and emission spectra on film of **Q′$_2$GaOC$_6$H$_4$CN**:TPD blend.*

The blended films **Q′$_2$GaOC$_6$H$_4$NO$_2$**:TPD, substantially are not chanced in absorption while a dramatic quenching of the emission intensity is observed (**Figure 6.15**).

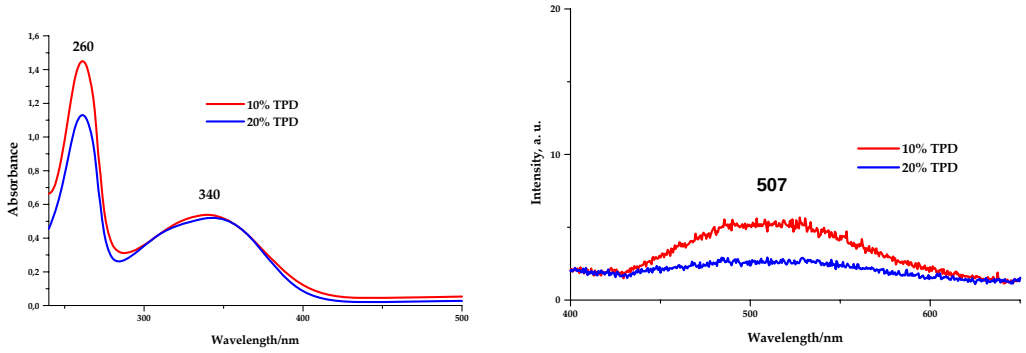

Figure 6.15: *absorption and emission spectra on film of Q'$_2$GaOC$_6$H$_4$NO$_2$:TPD blend.*

The blended film were studied also for the reference compound GaQ'$_3$. As shown in **Figure 6.16** the emission of the blended films is quenched by increasing the TPD percentage.

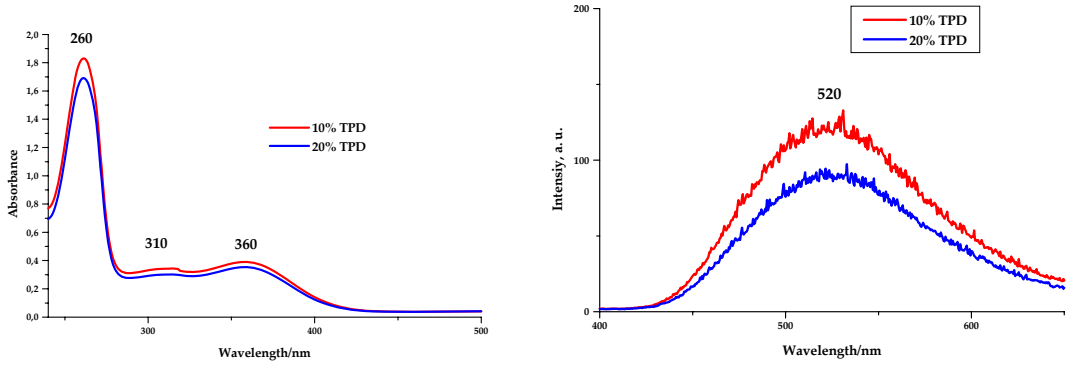

Figure 6.16: *absorption and emission spectra on film of GaQ'$_3$:TPD blend.*

6.1.3.3 Blended film with TPBI

The photophysical spectra on film obtained from blended dichloromethane solutions of **Q'$_2$GaOC$_6$H$_4$R** together with TPBI in 10% and 20% in weight.

In **Figure 6.17** are reported the absorption and the emission spectra of the **Q'$_2$GaOC$_6$H$_5$**:TPBI blend.

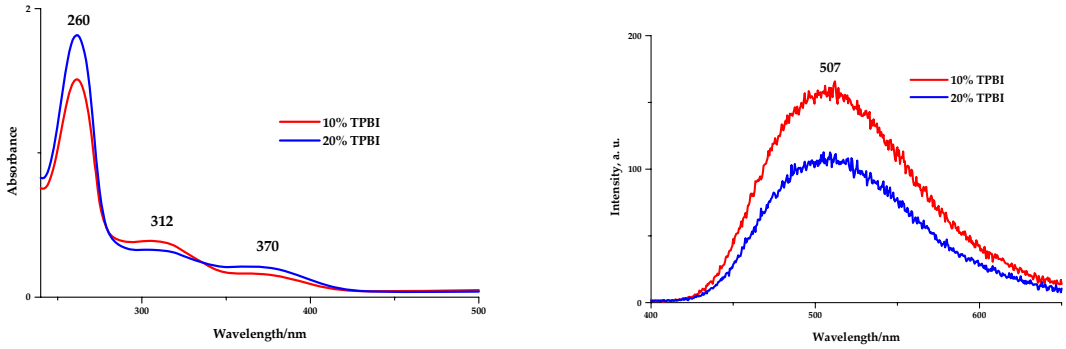

Figure 6.17: *absorption and emission spectra on film of* ***Q'₂GaOC₆H₅****:TPBI blend.*

In the absorption spectra the band intensity at 312 nm increase and the other one is shifted to 370 nm. The emission intensity is quenched by increasing the TPBI percentage. The same behaviour in absorption is observed for the **Q'₂GaOC₆H₄CN**:TPBI blended films (**Figure 6.18**).

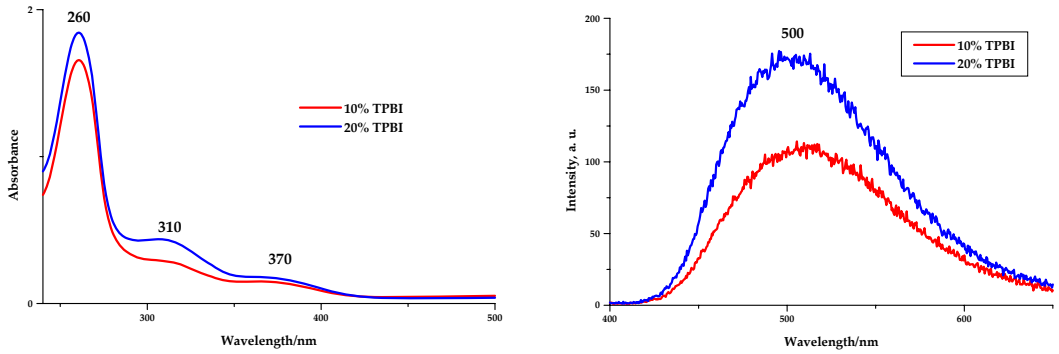

Figure 6.18: *absorption and emission spectra on film of* ***Q'₂GaOC₆H₄CN****:TPBI blend.*

The emission spectra show a strong enhancement of the emission intensity by increasing the TPBI percentage.

In the absorption spectra of **Q'₂GaC₆H₄NO₂**:TPBI a growing intensity is observed for the band at 315 while emission spectra (**Figure 6.19**) show the emission intensity increasing probably due to an energy transfer mechanism between TBPI and **Q'₂GaC₆H₄NO₂**.

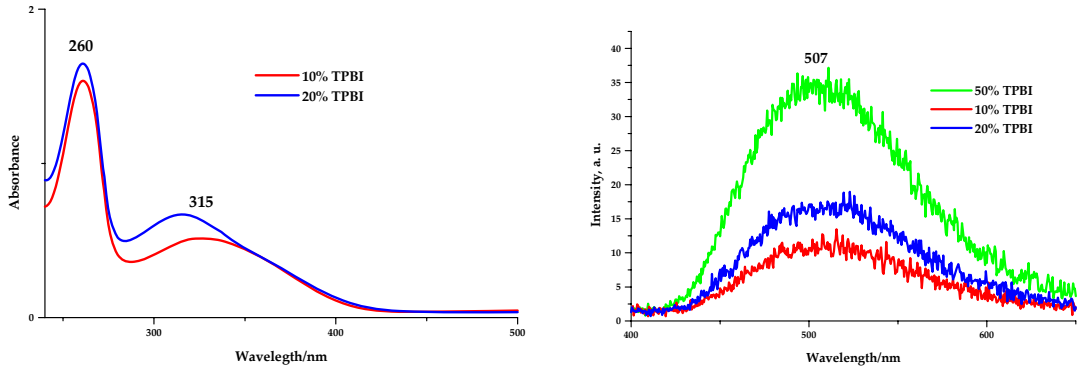

Figure 6.19: *absorption and emission spectra on film of* ***Q′₂GaOC₆H₄NO₂****:TPBI blend.*

The absorption and the emission spectra of the GaQ′$_3$:TPBI blended films are described in **Figure 6.20**.

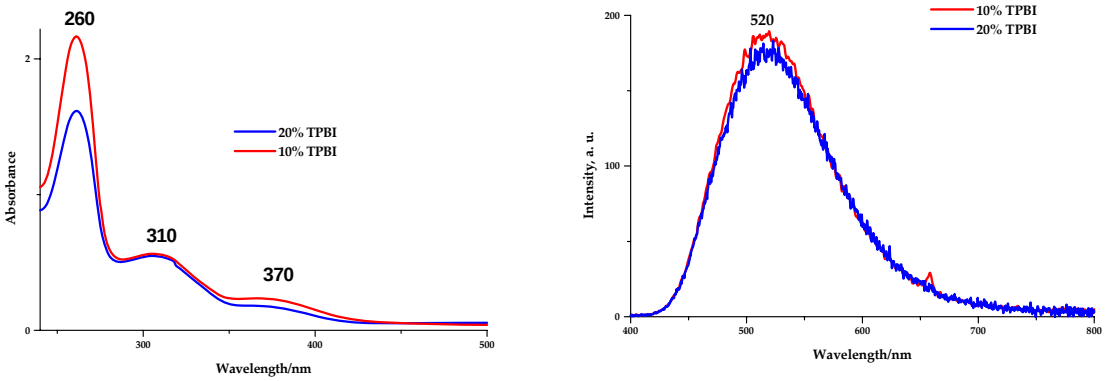

Figure 6.20: *absorption and emission spectra on film of GaQ′$_3$:TPBI blend.*

The absorption band at 310 nm is due to the TPBI contribution and the band at 360 nm is shifted at 370 nm. In the case of GaQ′$_3$ the increasing presence of the TPBI cause only a weak quenching of the emission intensity.

The behaviour of all blended film samples could be resumed in the **Scheme 6.2**. By increasing the percentage of TPD and TPBI in the blend the emission increase ↑ or the decrease ↓ the intensity**.**

	:TPD *Hole transporting material*	:TPBI *Electron transporting material*
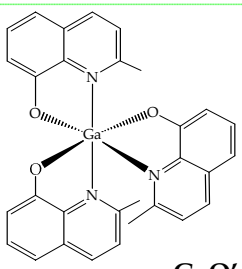 **GaQ′₃**	↓	↓ *Very weak quenching*
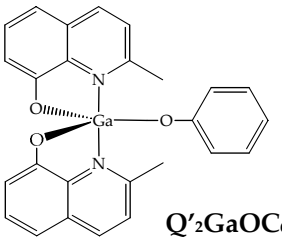 **Q′₂GaOC₆H₅**	**red shift 507 → 520 nm** ↑ *strong enhancement*	**507 nm** ↓
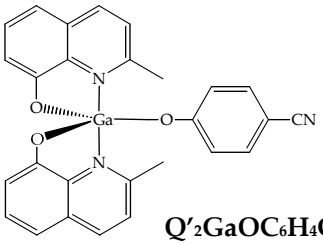 **Q′₂GaOC₆H₄CN**	**red shift 507 → 520 nm** ↓ *strong quenching*	**500 nm** ↑ *strong enhancement*
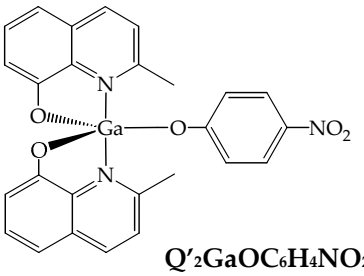 **Q′₂GaOC₆H₄NO₂**	**red shift 507 → 520 nm** ↓	**507 nm** ↑ *strong enhancement*

[a] λ_{ex} = 365 nm

Scheme 6.2: *blended film behaviour.*

The gallium complexes:TPD blended films show a strong red-shift of the emission maximum values, more than 10 nm, respect those of the not blended film as previously illustrated. The emission maximum values of the blended films obtained with TPBI are weakly red-shifted only **Q′₂GaOC₆H₄CN** blended films show exactly the same maximum emission value of not blended film.

6.2 Bimetallic gallium complexes obtained with bisphenol.

The gallium complex in which the monodentate ligand is a 4,4′-bisphenol **Q′$_2$GaOC$_6$H$_4$C$_6$H$_4$OGaQ′$_2$**, reported in **Figure 6.21**, was the only bimetallic compound obtained with high purity. Indeed the presence of unreacted 2-methyl-8-hydroxyquinoline and biphenol ligand or the presence of GaQ′$_3$ were observed as impurities in the absorption spectra.

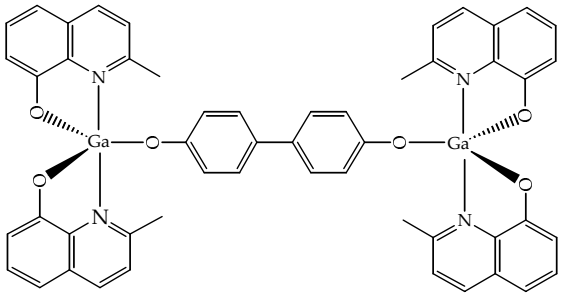

Figure 6.21: *Q′$_2$GaOC$_6$H$_4$C$_6$H$_4$OGaQ′$_2$ bimetallic gallium complex.*

Figure 6.22 illustrate the **Q′$_2$GaOC$_6$H$_4$C$_6$H$_4$OGaQ′$_2$** absorption and emission spectra collected in acetic acid solution. The intense bands at 260 nm and 360 nm show the typical spectral characteristics of the pentacoordinated gallium compounds with two 2-methyl-8-hydroxyquinolinate moieties. In **Table 6.5** are collected the photophysical data.

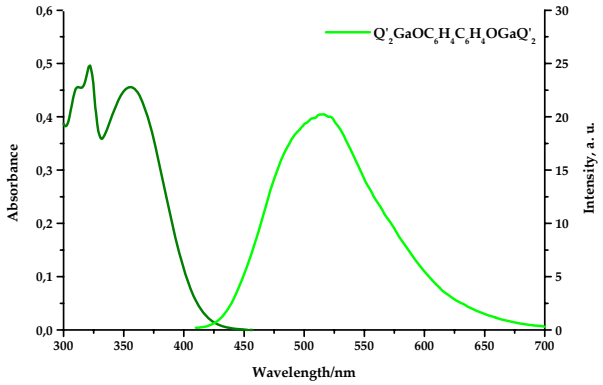

Figure 6.22: *absorption and emission bands of* ***Q′$_2$GaOC$_6$H$_4$C$_6$H$_4$OGaQ′$_2$.***

$Q'_2GaOC_6H_4C_6H_4OGaQ'_2$	***Absorbance*** λ***,nm*** *(ε, L mol⁻¹ cm⁻¹)*	***Emission*** λ***, nm*** , [a] Φ_{PL}
	320(36776) - 353 (9200)	520 (0.05)

[a] λ_{ex} = 365 nm

Table 6.5: *photophysical data of* $Q'_2GaOC_6H_4C_6H_4OGaQ'_2$.

The emission maximum value is red-shifted respect those displayed by the monometallic gallium compounds previously described. In particular very low photoluminescence quantum yield is revealed. Because of this compound show poor solubility, the characterization on film wasn't allowed.

6.3 Photophysical properties of $Q'_2GaL'^n$ compounds

The electronic states responsible of the emission are centred on the Q'_2Ga-fragment as discussed in the previous paragraph. A first observation of the photophysical data reported in literature about the $Q'_2GaOOCC_6H_5$ compound,[1] pentacoordinated gallium(III) complexes in which the pentacoordination is achieved with a carboxylate instead a phenoxyde, the spectral behaviour is retained while the photoluminescence quantum yield is reduced. Sapochak *et al*. attribute this quenching to the presence of the carbonyl group, known to cause fluorescence quenching.[1]

The absorption and the emission spectra of $\mathbf{Q'_2GaL'^n}$ gallium complexes, described in **Figure 6.23**, were collected in dichloromethane solutions.

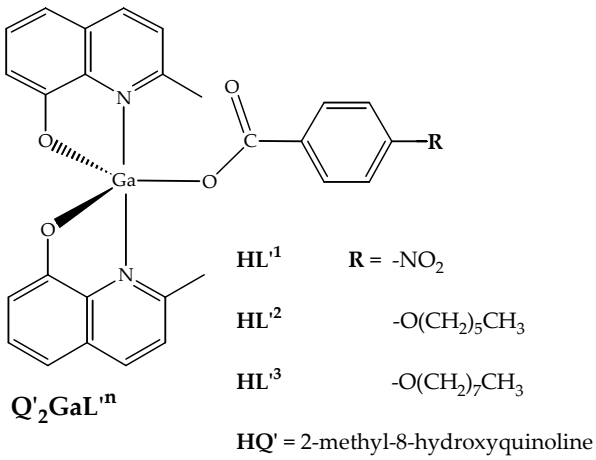

***Figure 6.23: Q′₂GaLₙ** compounds.*

Figure 6.24 report the absorption spectra of **Q′₂GaL′²** and **Q′₂GaL′³**.

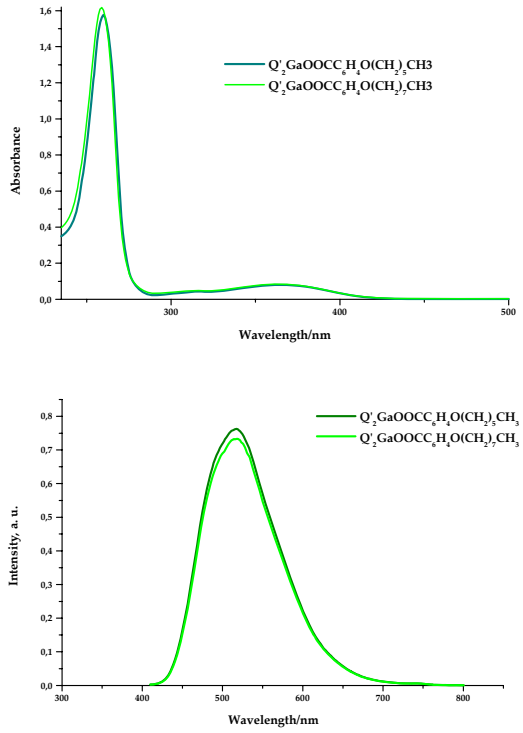

***Figure 6.24**: absorption and emission spectra of **Q′₂GaL′²** and **Q′₂GaL′³**.*

Absorption spectra show the typical intense bands centred at 260 nm and 365 nm due to the π–π* transitions. Emission bands are less broad than the emission of showed by gallium compounds obtained with phenoxyde ligands. **Q′₂GaOC₆H₄NO₂** graphs are not illustrated because of the very low intensity.

In **Table 6.6** are reported the collected data in which are included those of $Q'_2GaOOCC_6H_5$ compound reported in literature by Saphochak..

$Q'_2GaL'^n$	CH_2Cl_2 solutions		Film	
	Absorbance λ/nm, (ε/$M^{-1}cm^{-1}$)	Emission λ/nm (Φ_{PL})	Absorbance λ/nm	Emission λ/nm
$\mathbf{Q'_2GaOOCC_6H_5^1}$	366	500 (0.06)	/	/
$\mathbf{Q'_2GaOC_6H_4NO_2}$	260(23370) 315 (sh), 363(1100)	515 (0.08)	263 – 370	510
$\mathbf{Q'_2GaOOCC_6H_4O(CH_2)_5CH_3}$	260(14980) 315(2937) 365(4034)	515 (0.30)	263 – 370	505
$\mathbf{Q'_2GaOOCC_6H_4O(CH_2)_7CH_3}$	260(10231) 315(3062), 365(5250)	515 (0.40)	263 – 370	505

Table 6.6: *photophysical data of* $\mathbf{Q'_2GaL'^n}$ *in solution and on film.*

The maximum emission values in solution are red-shifted about 15 nm respect the compound reported by Sapochak. Films were obtained by spin-coating from dichloromethane solutions, the collected absorption spectra are slightly red shifted while a blue-shift of 10 nm is observed relatively to the compound with the alkylic chain in *p*-position of the benzoic ligand.

The excitation wavelength was 365 nm for $\mathbf{Q'_2GaL'^1}$ while was changed to 315 nm for $\mathbf{Q'_2GaL'^2}$ and $\mathbf{Q'_2GaL'^3}$. $\mathbf{Q'_2GaL'^1}$ shows Φ_{PL} value comparable with those reported in literature for $Q'_2GaOOCC_6H_5$ compound, contrarily to the expectations, strong enhancement is obtained with compound $\mathbf{Q'_2GaL'^2}$ and $\mathbf{Q'_2GaL'^3}$.

6.3.1 Photophysical data of $\mathbf{Q'_2GaL'^n}$ *compounds with trisubstrituted ligands*

The synthesised $\mathbf{Q'_2GaOOCC_6H_4(OC_6H_{13})_3}$ and $\mathbf{Q'_2GaOOCC_6H_4(OC_{14}H_{29})_3}$ compounds, illustrated in **Figure 6.25**, were characterised in dichloromethane solution and on film obtained by spin-coating techniques

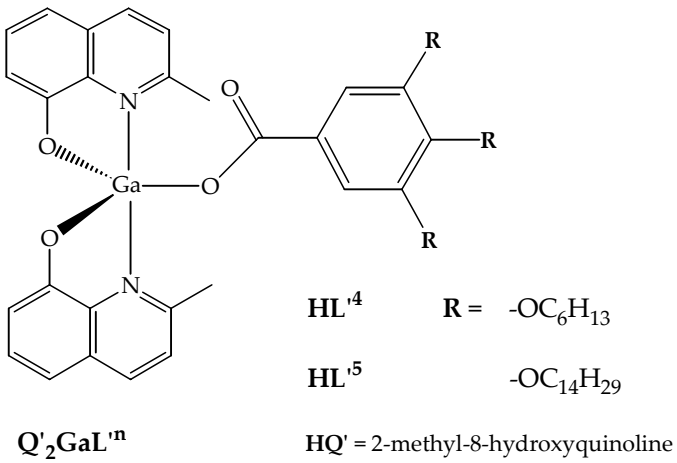

***Figure 6.25: Q′₂GaL′ⁿ** compounds.*

Absorption and emission spectra, reported in **Figure 6.26**, exhibit the typical spectral profile of this class of pentacoordinated compounds.

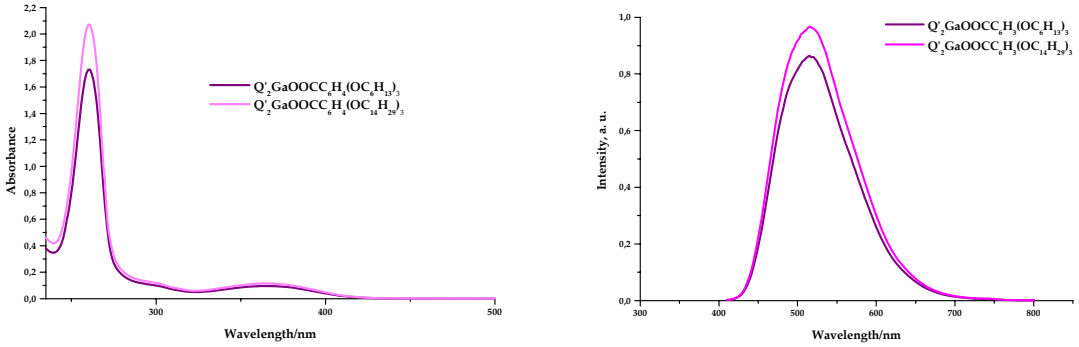

***Figure 6.26:** absorption spectra of **Q′₂GaL′ⁿ**.*

This series of complexes, obtained with trisubstituted benzoic acids derivatives, shows in the absorption spectra the presence of a band at 300 nm with almost the same extinction coefficient, ε, of the band at 365 nm, the emission spectra were registered exciting both the solutions and the film at 300 nm. The maximum emission values are centred around 515 nm while a strong blue-shift of 20 nm is revealed on film. Furthermore, high Φ_{PL} value are found for both compounds as described in **Table 6.7**.

$Q'_2GaL'_n$	CH_2Cl_2 solutions		Film	
	Absorbance λ/nm, ($\varepsilon/M^{-1}cm^{-1}$)	*Emission* λ/nm (Φ_{PL})	*Absorbance* λ/nm	*Emission* λ/nm
$Q'_2GaOOCC_6H_4(OC_6H_{13})_3$	260(167479) 300(9024) 365(9268)	515 (0.50)	263 – 370	495
$Q'_2GaOOCC_6H_4(OC_{14}H_{29})_3$	260(88717) 300(4769) 365(4770)	515 (0.40)	263 – 370	495

Table 6.7: *collected photophysical data of* $Q'_2GaL''_n$.

6.3.2 Photophysical data of bimetallic compounds

The photochemical behaviour of this series of compounds, **Figure 6.27**, correspond to the observation previously evidenced. **Table 6.8** report the collected data.

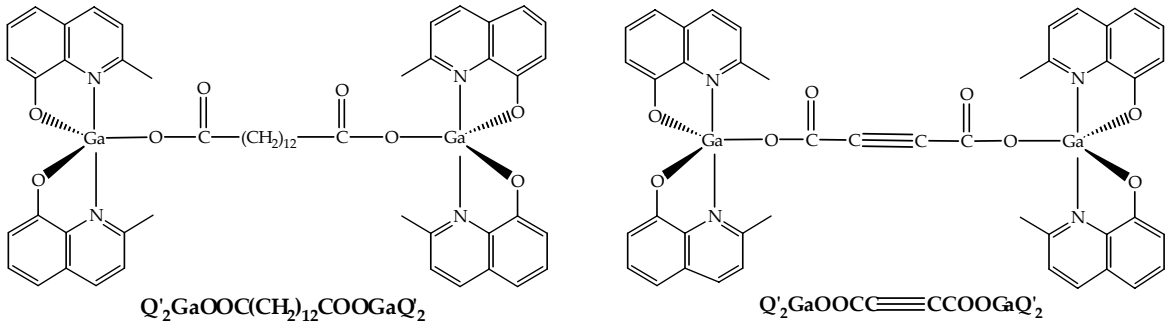

Figure 6.27: *synthesised bimetallic compounds*.

Compound $Q'_2GaOOC(CH_2)_{12}COOGaQ'_2$ bearing the alkylic chain as a flexible spacer between the two chromophores show better photoluminescence quantum efficiency values than $Q'_2GaOOCC{\equiv}CCOOGaQ'_2$. The structure of this last one was reported in literature, but photophysical data are not reported.

Compound	*CH_2Cl_2 solutions*		*Film*	
	Absorbance ***λ/nm,*** *(ε/$M^{-1}cm^{-1}$)*	***Emission*** ***λ/nm*** *($^a\Phi_{PL}$)*	***Absorbance*** ***λ/nm***	***Emission*** ***λ/nm***
Q'$_2$GaOOCC≡CCOOGaQ'$_2$	260(111150) 296(2830),315(3620) 365(6580)	517 (0.20)	265 – 370	500
Q'$_2$GaOOC$(CH_2)_{12}$COOGaQ'$_2$	260(68730) 300(1890), 315(2400) 364 (3600)	512 (0.36)	263 – 370	510

Table 6.8*: collected data of bimetallic compounds.*

6.4 Polymetallic gallium compounds

The word porphyrin derive from the Greek word *porphura* meaning purple, and all porphyrins are intensely coloured. The study of this kind of molecular species involve a lot of attention because of their interesting photophysical properties. Thus, combining chemical synthetic versatility and electro-optical properties of these molecules, many assembled structures are synthesised and are under investigation to emulate at molecular level light-harvesting complexes and reaction centres of natural photosynthesis. Furthermore, in a bottom –up approach, the target is to build optoelectronic devices as switches, wires, logic element, information storage. Porphyrins can be considered ideal components to construct supramolecular systems due to the rigid and planar geometries, intense absorption bands in the visible region, relatively long fluorescence decay time, facile tunability of their optical and redox properties by metalation / functionalization.[13]

For these reasons **H_2TPP(OH)$_4$** and **H_2TPP(COOH)$_4$** were chosen in order to study the optoelectronic properties of the synthesised polymetallic

ZnTPP(OGaQ′$_2$)$_4$ and **ZnTPP(COOGaQ′$_2$)$_4$** compounds described in **Figure 6.28.**

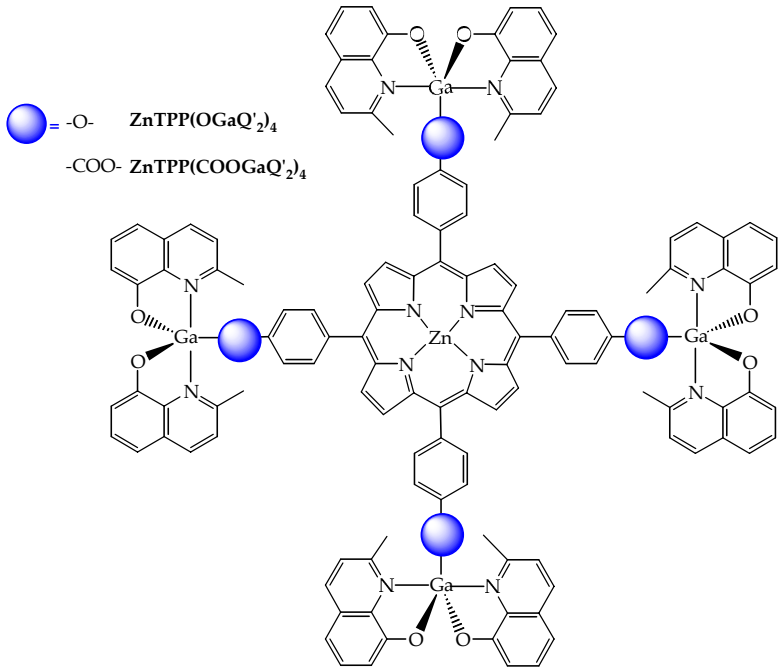

Figure 6.28: *polymetallic* ***ZnTPP(OGaQ′$_2$)$_4$*** *and* ***ZnTPP(COOGaQ′$_2$)$_4$*** *compounds.*

The electronic absorption spectra of **H$_2$TPP(OH)$_4$** and **H$_2$TPP(COOH)$_4$** is typical of a porphyrin. Its consist of a strong transition to the second excited state ($S_0 \rightarrow S_2$) at about 418 nm called Soret or B band and the four weak vibrational transitions to the first excited state ($S_0 \rightarrow S_1$) ranging from 516 nm to 650 nm, named Q bands. Both transitions are $\pi \rightarrow \pi^*$ as illustrated by Gauterman four orbital model. Further, the phenols or the benzoic units at the *meso* positions form with the porphyrin ring a large dihedral angle which prevent a satisfactory π-electron delocalization.[14] Such a conformation prevents the intermolecular π–π interactions among porphyrin cores which for unsubstitued porphyrins usually quench the fluorescence emission, and in thin solid film is responsible of degradation due to aggregation phenomena. Although at high concentrations they show an appreciable fluorescence.[15]

The polymetallic gallium compounds obtained with porphyrins were studied in methanol solutions and the photoluminescent quantum yield was calculated using cresyl violet perchlorate (CV) (MeOH, Φ_{PL}= 0,54) as standard.

6.4.1 Photophysic study of ***ZnTPP(OGaQ'$_2$)$_4$***

Figure 6.29 report the absorption spectra of **H_2TPP(OH)$_4$**, **ZnTPP(OH)$_4$** and **ZnTPP(OGaQ'$_2$)$_4$** collected in methanolic solutions.

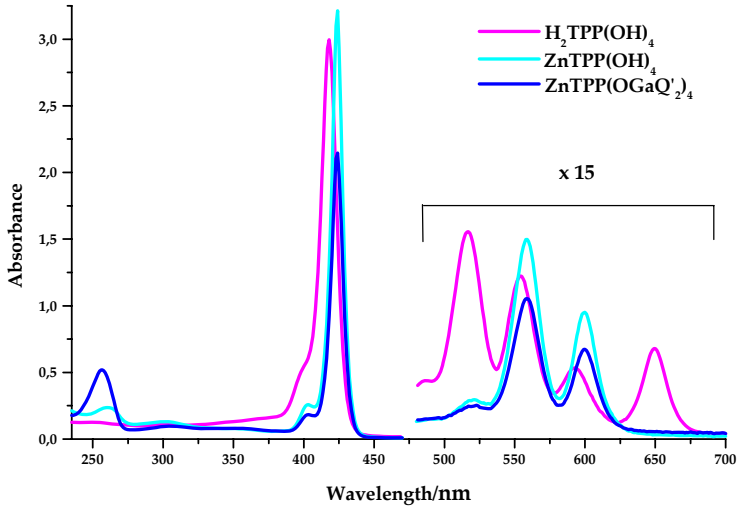

Figure 6.29: H_2TPP(OH)$_4$, ZnTPP(OH)$_4$ and ZnTPP(OGaQ'$_2$)$_4$ absorption spectra.

Comparing the absorption spectra of **H_2TPP(OH)$_4$** and **ZnTPP(OH)$_4$**, it is possible to observe the slightly B band red-shift, and a change in the Q band. In fact the band intensity at 500 nm is strongly reduced and the band at 650 nm disappear. This behaviour is retained in **ZnTPP(OGaQ'$_2$)$_4$** absorption spectra. In that case the contribution of the *Q'$_2$Ga-* fragment is evidenced by the typical intense band centred at 256 nm, and a less intense absorption at 358 nm, both assigned to π–π* transitions localized on the *Q'$_2$Ga-* fragment.

The introduction of a metal cation, in that case zinc, can be detected by UV analysis. The conformation of porphyrin macrocycle is influenced by the

complexed central cavity and by the substituents in *meso* positions. So a square planar conformation is preferred. The simplification of the absorption spectra is due to symmetry enhancement of the porphyrin macrocycle.[16-18]

Emission spectra were recorded in methanol with excitation wavelenght of 350 nm. The spectra reported in **Figure 6.30** show the intense emission bands of **H_2TPP(OH)$_4$** at 658 nm and 720 nm due to vibronic deactivation $S_1 \rightarrow S_0$. Because of the internal conversion from S_2 to S_1 is rapid, fluorescence can only be detected from S_1.

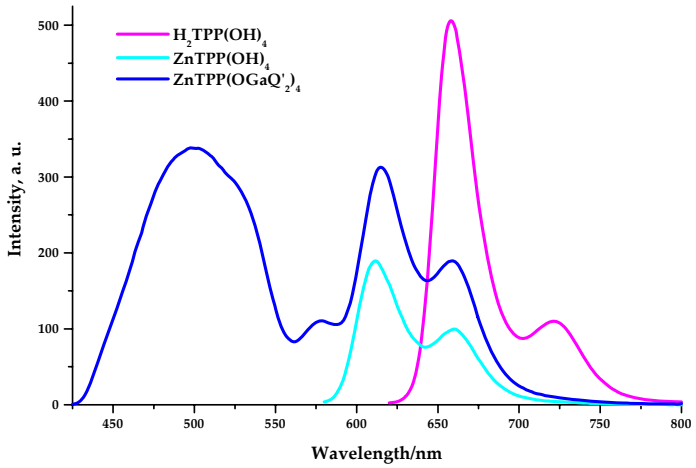

Figure 6.30: H_2TPP(OH)$_4$, ZnTPP(OH)$_4$ and ZnTPP(OGaQ′$_2$)$_4$ emission spectra.

The zinc presence in **ZnTPP(OH)$_4$** influence a strong blue-shift of the emission maximum values about 60 and 48 nm respectively. In the emission spectrum of **ZnTPP(OGaQ′$_2$)$_4$** complex it is possible to observe the contribution of the *Q′$_2$Ga*-fragments revealed with the broad emission band centred at 510 nm that can be attributed to a fluorescence deactivation (τ = 12.5 ns) from the lowest electronic excited state. Furthermore, the intense bands at 614 nm and 657 nm are attributed to the zinc porphyrinic moiety. **Figure 6.31** report the deconvolution of the **ZnTPP(OGaQ′$_2$)$_4$** emission spectrum in the two components **ZnTPP(OH)$_4$** and **Q′$_2$GaOC$_6$H$_5$**.

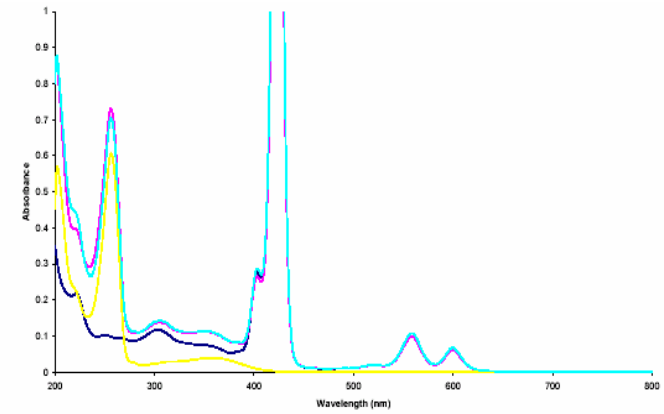

Figure 6.31: *deconvolution of the* ***ZnTPP(OGaQ′$_2$)$_4$*** *spectrum.*

Figure 6.32 shows the deconvolution of the **ZnTPP(OGaQ′$_2$)$_4$** spectrum in the two components **ZnTPP(OH)$_4$** and **Q′$_2$GaOC$_6$H$_5$**.

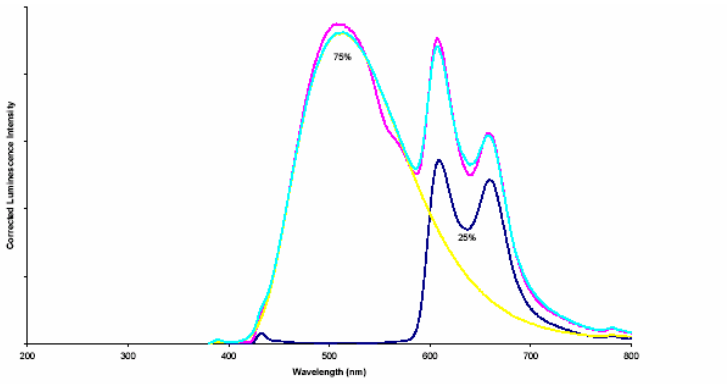

Figure 6.32: *deconvolution of the* ***ZnTPP(OGaQ′$_2$)$_4$*** *emission spectrum.*

In **Table 6.9** are reported the lifetimes τ and the photoluminescence quantum yields of **H$_2$TPP(OH)$_4$**, **ZnTPP(OGaQ′$_2$)$_4$** and of **Q′$_2$GaOC$_6$H$_5$** as reference compound.

Compound	Absorption λ_{max}/nm (ε/$M^{-1}cm^{-1}$)	Emission [a] λ_{max} /nm	Φ_{PL}	τ/ns
$H_2TPP(OH)_4$	424(555000), 559(18500) 600(11500)	610	0.018	1.2
$ZnTPP(OGaQ'_2)_4$	256(210000), 352(33000) 424(931000), 559(29500) 600(18500)	500, 605	0.040	12.4[b] 1.2 (64%), 11.7 (36%)[c]
$Q'_2GaOC_6H_5$	256(67000), 358(4500)	510	0.106	12.5

In methanol at room temperature; [a] λ_{ex} = 350 nm; [b] λ_{em} = 500 nm; [c] λ_{em} = 605 nm.

Table 6.9: *photophysical data and life time τ of $H_2TPP(OH)_4$, $ZnTPP(OGaQ'_2)_4$ and $Q'_2GaOC_6H_5$.*

6.4.1.1 Energy transfer properties

If the absorption spectrum of **$ZnTPP(OH)_4$** and **$Q'_2GaOC_6H_5$** are compared as suggested in **Figure 6.33**, it can be noted an overlap region around 500 nm suggesting a Franck-Condon factor that experimentally is proportional to a spectral overlap integral between the emission of the donor an the absorption of the acceptor.

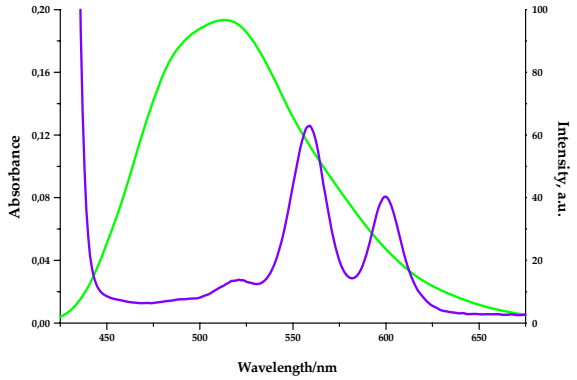

Figure 6.33: *Overlap of the absorption spectrum of $ZnTPP(OH)_4$ (blu line) with the emission spectrum of $Q'_2GaOC_6H_5$ (green line).*

Due to such features an energy transfer (ET) mechanism from the donor (**D**) **Q′$_2$GaOC$_6$H$_5$**, to the acceptor (**A**) **ZnTPP(OH)$_4$**, could be expected in **ZnTPP(OGaQ′$_2$)$_4$**. So the polymetallic species could be considered as if is an antenna system where the **D** and **A** chromophores are covalently linked then schematically represented as a simple dyad **D**-B-**A** where B, the chemical linker. In the present study B can be seen as a phenol bearing in *para* position the porphyrin macrocycle.

In principle, the Dexter ET should be ineffective in **ZnTPP(OGaQ′$_2$)$_4$**, since, as previously mentioned, the phenol rings, with respect to the porphyrin ring, adopt a tilted conformation which hampers a consistent orbital overlap between the **D** and **A** sites. Indeed, as shown by luminescence spectrum of **ZnTPP(OGaQ′$_2$)$_4$** (**Figure 6.34**)

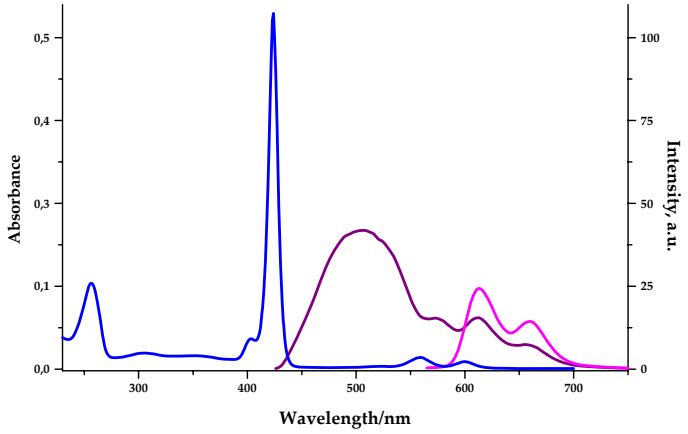

Figure 6.34: *absorption and emission spectra of* ***ZnTPP(OGaQ′$_2$)$_4$***

the presence of a band at 500 nm (λ_{ex} = 256 nm), is certainly attributable to the emission of the **D** component (*Q′$_2$Ga-* fragment), while exciting at 424 nm only the emission of the porphyrinic moiety is obtained. Then complete ET process from **D** to **A** can be excluded. Alternatively, taking into account the Förster mechanism, it should be recalled that the transfer efficiency can be calculated according to the formula $E_{RET} = 1 - (\tau_{DA}/\tau_D)$, wherein τ_{DA} and τ_D are the lifetimes of

D, respectively with and without **A**. The lifetimes measured at the emission maxima, 500 nm for **ZnTPP(OGaQ′$_2$)$_4$** (τ_{DA} = 12.4 ns) and 510 nm for **Q′$_2$GaOC$_6$H$_5$** (τ_D = 12.5 ns), from these data E_{RET} results 0.008, a value which suggests that in **ZnTPP(OGaQ′$_2$)$_4$** the RET mechanism, probably because of the unfavourable κ^2 factor, practically does not work.[19] If an energy transfer mechanism is not favoured, **ZnTPP(OGaQ′$_2$)$_4$** exhibit two emission colours. By choosing the right excitation wavelength it is possible to tune from the *Q′$_2$Ga*-lateral pendant emission to the porphyrinic core emission.

*6.4.2 Photophysic study of **ZnTPP(COOGaQ′$_2$)$_4$***

Absorption and the emission spectra of **H$_2$TPP(COOH)$_4$** and **ZnTPP(COOH)$_4$** show the same photophysical behaviour described in the previous paragraph. The Q band at 646 nm disappear because of the presence of zinc in the central cavity of the porphyrin and the absorption spectra is red-shifted respect to those of **ZnTPP(OH)$_4$**. On the contrary **ZnTPP(COOGaQ′$_2$)$_4$** show in absorption again the presence of four Q bands (**Figure 6.35**). This evidence could arise from conformational distortion of the structure probably due to some flexibility induced by the presence of carboxylates.

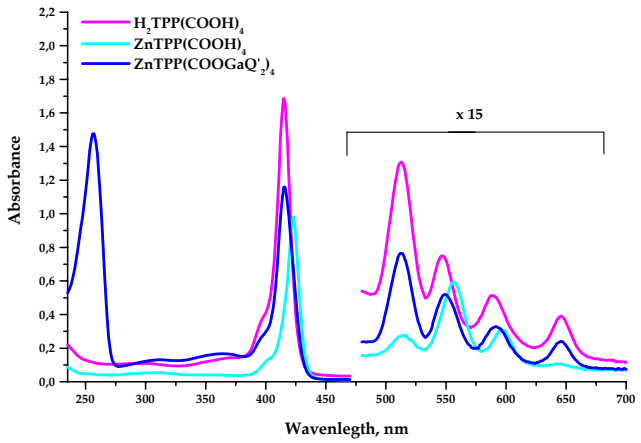

***Figure 6.35**: absorption spectra of **H$_2$TPP(COOH)$_4$**, **ZnTPP(COOH)$_4$** and **ZnTPP(COOGaQ′$_2$)$_4$**.*

In **Figure 6.36** are reported the emission spectra collected in methanol solutions. The emission bands of all species are shifted to lower frequencies respect those of the phenol substituted porphyrins derivatives previously described.

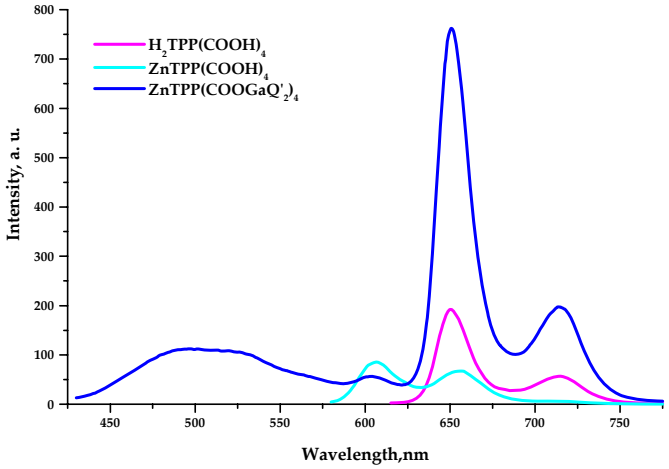

Figura 6.39: emission spectra of ***H2TPP(COOH)4, ZnTPP(COOH)4*** *and* ***ZnTPP(COOGaQ'2)4.***

Table 6.10 report the photophysical data of all compounds. Unlikely the extinction coefficients ε are not calculated because of the poor solubility of all these molecular species.

Compounds	***Absorbance*** λ_{max} ***/nm***	***Emission*** λ_{max} ***/nm***	Φ_{PL}
H2TPP(COOH)4	240, 300, 370, 398, 415 512, 547, 588, 646	650, 715	0.012
ZnTPP(COOH)4	310, 358, 400, 422 514, 556, 596	607, 656	0.015
ZnTPP(COOGaQ'2)4	256, 310, 364, 400, 420 513, 550, 591, 646	500, 603 650, 715	0.13

Table 6.10: *photophysical data of* ***H2TPP(COOH)4, ZnTPP(COOH)4*** *and* ***ZnTPP(COOGaQ'2)4.***

6.5 Conclusions

All pentacoordinated compounds are luminescent. The *Q'₂Ga–* fragment is slightly influenced by the presence of both mono-, bi- or polydentate ligand. As can be observed the absorption and the emission spectra retain almost the same spectra profile both in solution and in the solid state showing intense absorption bands in solution at 260 nm and at around 365 nm due to the $\pi \rightarrow \pi^*$ transitions. Emission maxima in solution ranging from 500 nm to 517 nm. Between these two absorption maxima a presence of a shoulder ranging from 300 nm to 315 nm differentiate the series of mono- and bimetallic compounds. **Q'₂GaLⁿ** compounds are good emitter. Φ_{PL} values ranging from 25% for **Q'₂GaOC₆H₄NO₂** to 44% for **Q'₂GaOC₆H₄CN**. The calculation of the electronic state reveal that all the reported orbitals are localized on the ligands, with a very small contribution from the metal centre. The presence of the electron attracting groups -CN and -NO_2 in the L^2 and L^3 ligands, leads to a stabilization of the p orbitals. In the case of **Q'₂GaOC₆H₅** (**1**), the HOMO is localized on L^1 (p_2), while the LUMO is localized on the Q' ligands (q_2). This characteristic is not retained in the case of **Q'₂GaOC₆H₄CN** (**2**) and **Q'₂GaOC₆H₄NO₂** (**3**). Furthermore, the presence of a π orbital (p_3) was computed. This may explain the low Φ_{PL} values (5%) collected exciting at 304 nm associated to an electronic transition from the p_2 quinolinate-localized orbital to the p_3 orbital. The antibonding character of this one, located between the oxygen and nitrogen atoms of the -NO_2 group, is responsible of the low population of the electronic state. The computations confirm also the observation reported in literature about the transition process dominated by the *Q'₂Ga–* fragment. The materials behave in the same manner as thin solid film. In fact, the absolute photoluminescence quantum yield collected on film, at excitation wavelength of 325 nm, show the emission quenching of the **Q'₂GaOC₆H₄NO₂** compounds. HOMO-LUMO electronic states are responsible

of the charge transfer properties of the materials when an bias voltage is applied to a device. Thus, blended (in 10% and 20% in weigth) film with TPD (hole transporting material) and TPBI (electron transporting material) were characterised in order to understand the charge transport abilities of **Q′$_2$GaL^n** compounds. The results reveal that **Q′$_2$GaOC$_6$H$_4$CN** and **Q′$_2$GaOC$_6$H$_4$NO$_2$** seem to be better hole transport material while **Q′$_2$GaOC$_6$H$_5$** act as electron transport material.

The photophysical behaviour, centred on the quinolinate moieties is retained also in **Q′$_2$GaL′^{n}** compounds. The compounds bearing in the *p*-position an aliphatic chain show intense emission and high Φ_{PL} values ranging from 30% to 50%. This phenomenon may be attributed to an self organization of the molecule due to the aliphatic chains. But properly explanation of the results need more investigation.

The **ZnTPP(OGaQ′$_2$)$_4$** and **ZnTPP(COOGaQ′$_2$)$_4$** polymetallic compounds were characterised in order to study possible energy transfer mechanism between more than two chromophores in the same chemical structure. The study was focussed **ZnTPP(OGaQ′$_2$)$_4$** complex because of its good solubility. The absorption and the emission spectra reveal the contribution of both the cromophores *Q′$_2$Ga–* fragment and Zn-porphyrin. The calculated lifetimes, attributed to the transition on the two chromophores, coupled with the tilted conformation of the phenol rings, with respect to the porphyrin ring, hamper energy transfer mechanisms. It seem that the two chromophores are independent each other, then exciting a two different excitation wavelength, corresponding to electronic state of the chromophores it is possible to switch between to different emissions.

REFERENCES

1. L. S. Sapochak, P. E. Burrows, D. Garbuzov, D. M. Ho, S. R. Forrest, M. E. Thompson, *J. Phys. Chem.*, 1996, **100**, 17766;

2. S. Tan, B. Zhao, Y. Zou, Z. Xiao, X. Wang, G. Yu, Y. Liu, D. Zhu, *J. Mater. Sci.*, 2004, **39**, 1405.

3. La Deda, M.; Aiello, I.; Grisolia, A.; Ghedini, M.; Amati, M.; Lelj, F. *Dalton Trans.* **2006**, 330.

4. Sapochack, L. S.; Benincasa, F. E.; Schofield, R. S.; Baker, J. L.; Riccio, K. K. C.; Fogarty, D.; Kohlmann, H.; Ferris, K. F.; Burrows, P. E. *J. Am. Chem. Soc.* **2002**, *124*, 6119.

5. Kushto, G. P.; Iizumi, Y.; Kido, J. ; Kafafi, Z. H. *J. Phys. Chem. A* **2000**, *104*, 3670.

6. Halls, M. D.; Schlegel, H. B. *Chem. Mater.* **2001**, *13*, 2632.

7. Degli Esposti, A.; Brinkmann, M.; Ruani, G. *J. Chem. Phys.* **2002**, *116*, 798.

8. Amati, M.; Lelj, F. *Chem. Phys. Lett.* **2002**, *107*, 2560.

9. Greenham, N. C.; Samuel, I. D. W. et al., *Chem. Phys. Lett.* **1995**, *89*, 241

10. Greenham, N. C.; Friend, R. H.; Bradley, D. D. C. *Adv. Mater.* **1994**, *6*, 491.

11. Zhang, X. H.; Lai, Z. Q.; Wong, T. C.; Lee, C. s.; Kwong, H. L.; Lee, S. T.; Wu, S. K. *Chem. Phys. Lett.* **2000**, *320*, 77.

12. Cheng, L. F.; Hung, L. M.; Ding, X. M.; Gao, Z. Q.; Lee, C. S.; Lee, S. T. *Display* **2000**, *21*, 51.

13. Scandola, F.; Chiorboli, C., Prodi, A.; Iengo, E.; Alessio, E. *Coordination Chemistry Reviews* **2006**, *250*, 1471.

14. Anderson, H. L. *Chem. Commun.* **1999**, 2323.

15. Lensen, M. C.; van Dingenen, S. J. T.; Elemans, J. A. A. W.; Dijkstra, H. P.; van Klink, G. P. M.; van Koten, G.; Gerritsen, J. W.; Speller, S.; Nolte, R. J. M.; Rowan, A. E. *Chem. Commun.* **2004**, 762.

16. Macquet, J. P. ; Theophanides, T. *Can. J. Chem.* **1973**, *51*, 219.

17. Takeda, J.; Sato, M.; *Tetrahedron Letters* **1994**, *35*, 21, 3565.

18. Hováth, O.; Huszánk, R.; Valicsek, Z.; Lendvay, G. *Coord. Chem. Rev.* **2006**, *250*, 1792.

19. Lakowicz, J. R. *Principle of Fluorescent Spectroscopy* **1999**, 2nd Ed., Kluwer Academic/Plenum Publishers, New York.